Antiferromagnetic order and Kondo-lattice behavior in single-crystalline Ce_2RhSi_3

M. Szlawska,[1] D. Kaczorowski,[1] A. Ślebarski,[2] L. Gulay,[1,*] and J. Stępień-Damm[1]
[1]*Institute of Low Temperature and Structure Research, Polish Academy of Sciences, P.O. Box 1410, 50-950 Wrocław, Poland*
[2]*Institute of Physics, University of Silesia, 40-007 Katowice, Poland*
(Received 22 January 2009; revised manuscript received 16 March 2009; published 29 April 2009)

Single crystal of Ce_2RhSi_3 was investigated by means of x-ray diffraction, magnetization, electrical resistivity, and heat-capacity measurements. Moreover, its electronic structure was studied by cerium core-level x-ray photoemission spectroscopy. The results revealed that Ce_2RhSi_3 is an antiferromagnetic Kondo lattice due to the presence of stable trivalent Ce ions.

DOI: 10.1103/PhysRevB.79.134435 PACS number(s): 75.50.Ee, 71.27.+a, 75.30.Mb

I. INTRODUCTION

The majority of compounds of the type R_2TM_3, where R=rare-earth (RE) or U, T stands for a d-electron transition metal, and M is a p-electron element, crystallize with the hexagonal AlB_2-type structure or its derivative. These phases exhibit a large variety of physical properties that are predominantly related to the degree of atomic disorder and/or topological frustration in triangular magnetic sublattices.[1] Compounds in which T and M atoms jointly occupy same crystallographic positions commonly show behaviors typical of nonmagnetic atom-disorder spin-glasses (NMAD SGs).[2,3] Partially ordered alloys, i.e., those showing some superstructure in the atom distribution, often exhibit ferromagnetic cluster-glass properties.[1,4–6] In turn, the phases with all the constituent atoms located at their own specific positions in the unit cell typically have nonmagnetic ground states[4,7–15] or show long-range magnetic ordering.[16–18]

The series of ternary rare-earth silicides RE_2RhSi_3 was reported to crystallize with fully ordered hexagonal unit cells with both lattice parameters doubled with respect to the AlB_2 type.[19–21] Magnetic measurements revealed that these compounds order antiferromagnetically for RE=Gd, Tb, Dy, Ho, and Er and ferromagnetically for RE=Nd.[19] Moreover, the neutron-diffraction data confirmed collinear antiferromagnetic ordering for Tb_2RhSi_3, Ho_2RhSi_3, and Er_2RhSi_3, while indicated a ferromagnetic spiral for Nd_2RhSi_3.[20,22]

The Ce-based phase Ce_2RhSi_3 has attracted particular attention due to its intriguing magnetic and electrical transport properties. In the first literature report it was characterized as an antiferromagnet with the Néel temperature T_N=6 K,[19] but no evidence for any long-range magnetic order down to 2 K was found in neutron-diffraction experiment.[20] Subsequent magnetic susceptibility, electrical resistivity, and heat-capacity studies corroborated the ordered state below 6–7 K,[21,23] which was described based on the results of other neutron-diffraction experiment as a simple collinear arrangement of the Ce magnetic moments along the b axis of an orthorhombic magnetic unit cell.[21] The magnetic moment derived at 1.3 K by the neutron diffraction was $1.3\mu_B$ per Ce atom.[21]

Furthermore, the compound was found to exhibit behavior typical of strongly correlated electron systems, such as enhanced linear contribution to the specific heat, large negative value of the paramagnetic Curie temperature, and negative logarithmic slope in the electrical resistivity.[23] Most recently, Kondo-lattice character of polycrystalline Ce_2RhSi_3 was corroborated by the results of magnetic-susceptibility and electrical resistivity measurements performed under hydrostatic pressure.[24,25] These latter findings motivated us to undertake our own detailed investigations of Ce_2RhSi_3, yet for the first time on well-defined single crystals of this interesting compound.

II. EXPERIMENTAL DETAILS

Single crystal of Ce_2RhSi_3 was grown by the Czochralski pulling method in a tetra-arc furnace under ultrapure argon atmosphere. The starting components were high-purity elements (Ce-3N, Ames Laboratory, Rh-3N, Chempur, and Si-6N, Chempur). The obtained crystal was 4 mm in diameter and 20 mm in length. The specimens for x-ray analysis and for physical measurements were cut from this crystal using a wire saw.

Single-crystal diffraction data were collected on a KUMA Diffraction four-circle diffractometer equipped with a charge coupled device (CCD) camera using Mo $K\alpha$ radiation. Crystal structure refinement was performed employing the program SHELXL-97.[26] Details of the single-crystal data collection and the structure refinement are given in Table I.

A polycrystalline sample of La_2RhSi_3, used as a nonmagnetic counterpart to the cerium compound studied, was synthesized by arc melting the stoichiometric amounts of the elemental components (La-3N, Ames Laboratory, purity of Rh and Si as given above) in Ti-gettered argon atmosphere. The button was flipped over and remelted several times to ensure good homogeneity of the material. Quality of the obtained alloy was checked by x-ray powder diffraction on a Stoe powder diffractometer with Cu $K\alpha$ radiation and by energy dispersive x-ray analysis using a Phillips 515 scanning electron microscope equipped with an EDAX PV 9800 spectrometer. The structure refinement was done employing the program FULLPROF.[27]

Magnetic-susceptibility measurements were performed in the temperature range of 1.72–400 K and in magnetic fields up to 5 T using a Quantum Design superconducting quantum interference device (SQUID) magnetometer. The magnetization at 1.72 K was measured as a function of magnetic field up to 9 T employing a Quantum Design PPMS platform. The heat capacity was studied within the temperature interval of

 ©2009 The American Physical Society

TABLE I. Crystallographic and structure refinement data for Ce_2RhSi_3.

Compound	Ce_2RhSi_3
Space group	$P6/mmm$
Unit-cell dimensions	$a=8.2240(12)$ Å $c=4.2261(8)$ Å
Volume	247.53(7) Å^3
Formula weight	467.42 g/mol
Calculated density	6.271 g/cm^3
Absorption coefficient	21.913 mm^{-1}
θ range for data collection	20.84°–43.05°
Ranges in hkl	$-10\leq h\leq 15$ $-15\leq k\leq 10$ $-5\leq l\leq 8$
Reflections collected/unique	3760/337 [R(int)=0.0641]
Completeness to θ=43.05°	82%
Refinement method	full-matrix least squares on F2
Data/restrains/parameters	337/0/13
Goodness of fit on F^2	1.157
Final R indices [$I\geq 2\sigma(I)$]	R1=0.0405, wR2=0.1115
R indices (all data)	R1=0.0414, wR2=0.1125
Extinction coefficient	0.000(8)
Largest diff. peak and hole	3.051 and −2.230 e/Å^{-3}

0.35–300 K in magnetic fields up to 8 T using a Quantum Design PPMS platform. The temperature and field variations of the electrical resistivity were studied from 2 to 300 K in applied magnetic fields up to 9 T employing a Quantum Design PPMS platform. External magnetic field was applied perpendicular to the current flowing through the specimen. The x-ray photoelectron spectra were obtained with monochromatized Al $K\alpha$ radiation using a PHI 5700 ESCA spectrometer.

III. RESULTS AND DISCUSSION

A. Crystal structure

In the unit cell of AlB_2 (space group $P6/mmm$) the atoms are located at just two positions: Al at 1a (0, 0, 0) and B at 2d (2/3, 1/3, 1/2). As mentioned in Sec. I, many of R_2TM_3 ternaries adopt this simple structure with R atoms occupying the 1a sites, while T and M atoms sharing the 2d positions. In the case of Ce_2RhSi_3, however, previous reports indicated

TABLE II. Atomic coordinates and equivalent isotropic thermal displacement parameters (in Å$^2\times 10^3$) for Ce_2RhSi_3.

Atom	Site	x	y	z	U (eq)
Ce1	1a	0	0	0	13(1)
Ce2	3f	1/2	0	0	8(1)
Rh	2d	2/3	1/3	1/2	9(1)
Si	6m	0.8336(1)	0.1664(1)	1/2	9(1)

TABLE III. Anisotropic thermal displacement parameters for the atoms in Ce_2RhSi_3 (in Å$^2\times 10^3$).

	U11	U22	U33	U23	U13	U12
Ce1	10(1)	10(1)	18(1)	0	0	5(1)
Ce2	8(1)	8(1)	9(1)	0	0	4(1)
Rh	9(1)	10(1)	10(1)	0	0	5(1)
Si	7(1)	7(1)	13(1)	0	0	3(1)

that this compound crystallizes with a superstructure with full atomic order, in which the a and c lattice parameters are doubled with respect to the AlB_2 subcell. Two different atom distributions were proposed based on the results obtained in two independent investigations of single crystals of Er_2RhSi_3: (i) Ce1 at 2b (0, 0, 1/4), Ce2 at 6h (x, y, 1/4), Rh at 4f (1/3, 2/3, 0), Si at 12i (1/6, 1/3, 0) (space group $P\bar{6}2c$),[19] and (ii) Ce1 at 2b (0, 0, 1/4), Ce2 at 6h (x, 2x, 1/4), Rh at 4f (1/3, 2/3, z), Si at 12k (x, 2x, z) (space group $P6_3/mmc$).[28]

Unexpectedly, none of these structures was found to model the x-ray data collected in the present work for the Czochralski grown single crystal of Ce_2RhSi_3. While doubling the AlB_2 subcell in the basal hexagonal plane was clearly observed, no diffraction spots which would manifest doubling the c parameter were recorded. Nevertheless, the refined structure is also fully ordered. The obtained arrangement of the atoms is as follows: Ce1 at 1a (0, 0, 0) site, Ce2 at 3f (1/2, 0, 0) site, Rh at 2d (2/3, 1/3, 1/2) site, and Si at 6m (x, y, 1/2) site (for the free parameters see Table II). The atomic thermal displacement parameters are shown in Table III.

The crystal structure of single-crystalline Ce_2RhSi_3 is shown in Fig. 1. The rhodium and silicon atoms build a two-dimensional hexagonal networks separated by planes of cerium atoms, which build discrete Si_6 rings. The Rh atom has a trigonal-planar Si coordination at the Rh-Si distance of 2.3781(10) Å. The two crystallographically inequivalent Ce atoms possess hexagonal prismatic environments. The Ce1 atom is coordinated by twelve Si atoms with the Ce1-Si distance of 3.1752(8) Å, and the Ce2 atom has four Rh nearest neighbors at the Ce2-Rh distance of 3.1782(4) Å and eight

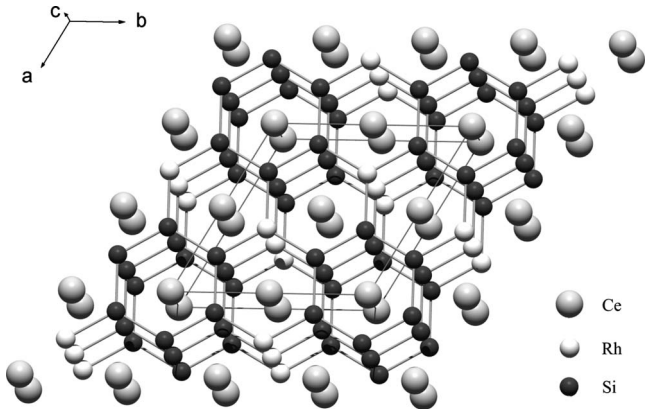

FIG. 1. Crystal structure of Ce_2RhSi_3.

TABLE IV. Interatomic distances in the Ce_2RhSi_3 unit cell (in Å).

Ce1	12	Si	3.1752(8)
	2	Ce1	4.2260(8)
	6	Ce2	4.1120(6)
Ce2	4	Rh	3.1782(4)
	8	Si	3.1797(5)
	2	Ce1	4.1120(6)
	4	Ce2	4.1120(6)
	2	Ce2	4.2260(8)
Rh	3	Si	2.3781(10)
	6	Ce2	3.1782(4)
Si	2	Si	2.3700(10)
	1	Rh	2.3781(10)
	2	Ce1	3.1752(8)
	4	Ce2	3.1797(5)

Si next-nearest neighbors at the Ce2-Si distance of 3.1797(5) Å. All these bond lengths are close to the sums of the respective covalent radii. The list of other interatomic distances is given in Table IV.

The refined structure of Ce_2RhSi_3 is closely related to that determined for U_2RuSi_3.[9] However, on the contrary to the latter prototype, in which the Si atoms occupy a general position $12o$ (x, y, z), in Ce_2RhSi_3 these atoms are coplanar with the transition-metal atoms, as reported before for the compounds Ce_2CoSi_3 and Eu_2PdSi_3.[10,29]

B. Magnetic properties

Figure 2 shows the temperature dependencies of the reciprocal magnetic susceptibility of single-crystalline Ce_2RhSi_3, measured in magnetic field applied parallel to the two principal hexagonal axes. Above about 200 K both susceptibility components follow the Curie-Weiss law with the

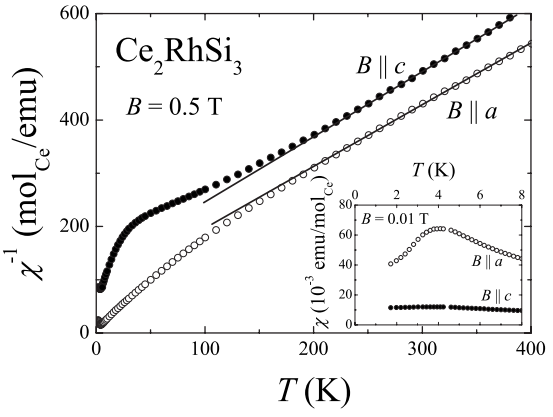

FIG. 2. Temperature dependencies of the reciprocal molar magnetic susceptibility of Ce_2RhSi_3, measured with magnetic field of 0.5 T oriented parallel to the a and c axes. Solid lines represent fits of the Curie-Weiss law to the experimental data above 200 K. Inset displays the magnetic-susceptibility components, measured at low-temperatures in a field of 0.01 T.

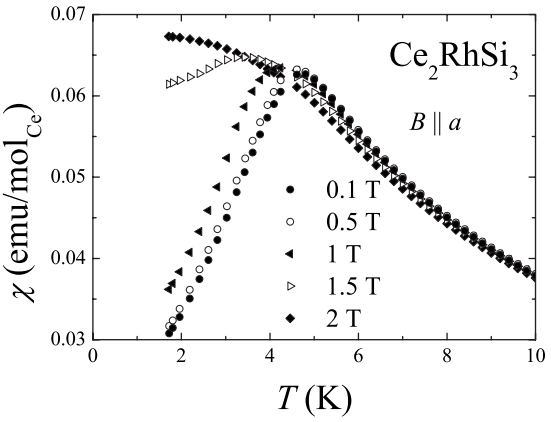

FIG. 3. Low-temperature magnetic susceptibility of Ce_2RhSi_3 measured in various magnetic fields applied along the a axis.

parameters: $\mu_{\text{eff}}^c = 2.55\mu_B$ and $\theta_p^c = -102$ K for $B \| c$ and $\mu_{\text{eff}}^a = 2.6\mu_B$ and $\theta_p^a = -78$ K for $B \| a$. The values of the effective magnetic moment μ_{eff} are very close to that expected for trivalent Ce ions ($2.54\mu_B$). In turn, the large negative values of the paramagnetic Curie temperature θ_p ($|\theta_p| \gg T_N$) may manifest hybridization of the $4f$ electronic states with the conduction band. Below 200 K, one observes distinct deviations from the Curie-Weiss behavior which probably occur due to gradual depopulation of the crystal-field levels.

As is apparent from the inset to Fig. 2, the studied single crystal of Ce_2RhSi_3 orders antiferromagnetically at $T_N = 4.5$ K. This ordering temperature is considerably different from $T_N = 6-7$ K, reported before for polycrystalline samples.[21,23,24] From the huge magnetic anisotropy observed in the ordered state, with χ_c being much smaller than χ_a and showing hardly any anomaly at T_N, one may conclude that the magnetic moments are confined in the ordered state to the hexagonal basal plane. This finding is in accord with the neutron-diffraction data obtained for the polycrystals.[21] With increasing the magnetic field strength the maximum in $\chi_a(T)$ shifts toward lower temperatures and strongly broadens, while above 1.5 T it is not discernible (see Fig. 3). The overall behavior of χ_a is reminiscent of antiferromagnets showing a field-induced metamagnetic transition.

At first glance, the metamagneticlike character of Ce_2RhSi_3 seems corroborated by the results of the magnetization measurements performed in the ordered region as a function of the magnetic field. The exemplary isotherms taken at $T = 1.8$ K are shown in Fig. 4. The $\sigma_a(B)$ curve (measured in the field applied parallel to the a axis) reveals a distinct anomaly near $B_c = 1.5$ T, in perfect agreement with the features observed for χ_a. It is, however, worthwhile noting that above B_c the magnetization remains nearly proportional to the magnetic field strength, in a manner typical for antiferromagnets, and only in fields stronger than 6 T does σ_a show a tendency to saturate. This feature implies that the anomalies at B_c manifest a change in the antiparallel arrangement of the magnetic moments in Ce_2RhSi_3 with respect to the direction of the external magnetic field, and thus it is rather not associated with the onset of field-induced ferromagnetic state, which is typically observed in metamagnetic systems. The $\sigma_a(B)$ isotherm (for $B \| c$) exhibits a straight-

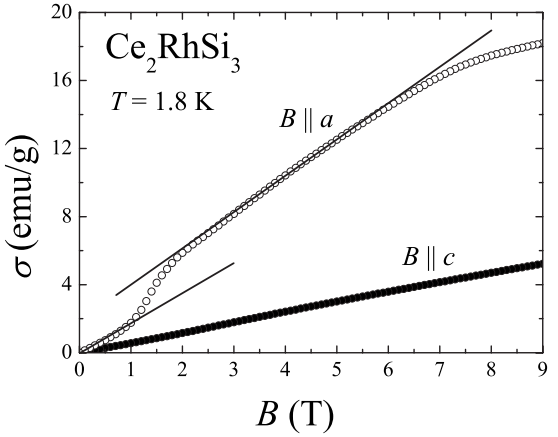

FIG. 4. Magnetic field variations of the magnetization in Ce_2RhSi_3, measured at 1.72 K with field applied along the two characteristic directions. Solid lines emphasize straight-line behaviors below and above $B_c = 1.5$ T.

line behavior up to the strongest fields applied, in line with the large magnetocrystalline anisotropy. For both directions of the magnetic field the magnetization was fully reversible, i.e., no hysteresis effect was observed.

In contrast with the Ce-based compound, La_2RhSi_3 is a weak Pauli paramagnet with nearly temperature-independent magnetic susceptibility of about 2×10^{-5} emu/mol at room temperature.

C. Specific heat

Figure 5 presents the temperature dependencies of the specific heat of Ce_2RhSi_3 and its nonmagnetic counterpart La_2RhSi_3. The solid line through the experimental points for the latter compound is the least-squares fit to the formula

$$C = C_{\mathrm{el}} + C_{\mathrm{ph},D} + C_{\mathrm{ph},E}, \tag{1}$$

in which the first term represents the electronic contribution in the form $C_{\mathrm{el}} = \gamma T$, while the other two terms are the

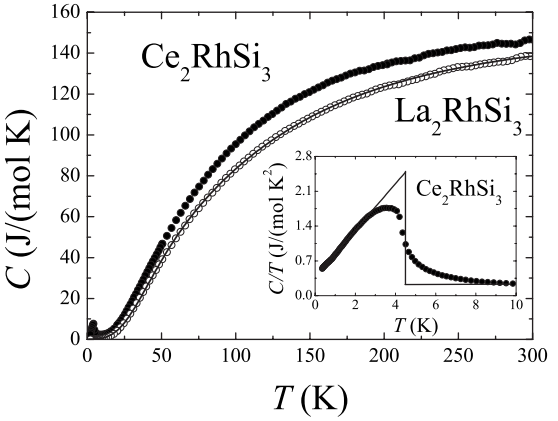

FIG. 5. Temperature variations of the specific heat of Ce_2RhSi_3 and La_2RhSi_3. Solid line is a fit described in the text. Inset presents the specific heat over temperature ratio for Ce_2RhSi_3 below 10 K. The idealized phase transition marked by the solid line has a step at $T_N = 4.5$ K.

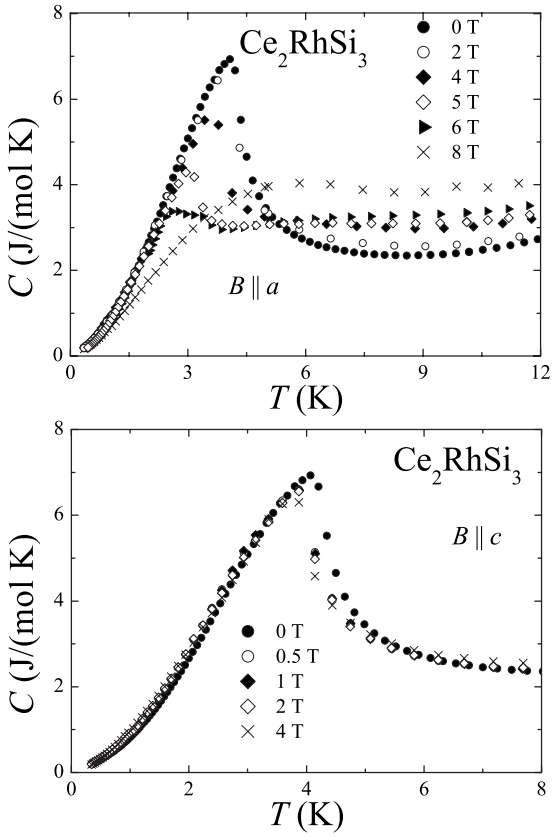

FIG. 6. Low-temperature specific heat of Ce_2RhSi_3 measured in several applied magnetic fields oriented along the a axis (upper panel) and the c axis (lower panel) of the hexagonal unit cell.

phonon contributions within the Debye and Einstein models, respectively. The acoustic modes, represented as Debye oscillators, contribute to the total specific heat as $C_{\mathrm{ph},D}(T) = 9Rn_D(T/\Theta_D)^3 \int_0^{\Theta_D/T} \frac{x^4 \exp(x)}{[\exp(x)-1]^2} dx$, while the optical modes are given by the Einstein formula $C_{\mathrm{ph},E}(T) = 3Rn_E \frac{(\Theta_E/T)^2 \exp(\Theta_E/T)}{[\exp(\Theta_E/T)-1]^2} dx$, where R is the gas constant, Θ_D, Θ_E, n_D, and n_E are the Debye temperature, the Einstein temperature, the number of Debye oscillators, and the number of Einstein oscillators, respectively.[30] For La_2RhSi_3 it was assumed that the Debye model properly describes vibrations of the Rh and Si atoms (i.e., $n_D = 12$), while the Einstein model is appropriate for the La atoms (i.e., $n_E = 6$). With these input parameters the specific heat of the compound can be well described by Eq. (1) (see Fig. 5) and the so-derived fit parameters are as follows: $\gamma = 4$ mJ mol^{-1} K^{-2}, $\Theta_D = 247$ K, and $\Theta_E = 522$ K.

The specific heat of Ce_2RhSi_3 is dominated at low temperatures by a saw-tooth-shaped anomaly at the antiferromagnetic phase transition. Using an equal entropy construction (see the inset to Fig. 5) the Néel temperature was estimated to be 4.5 K, in good agreement with the magnetic-susceptibility data. The observed broadening of the antiferromagnetic peak in $C(T)$ may be due to Kondo fluctuations of characteristic energy scale comparable to T_N (see below). As displayed in Fig. 6, upon applying external magnetic field along the a axis the anomaly in $C(T)$ shifts toward lower temperatures and its magnitude diminishes, in a manner typi-

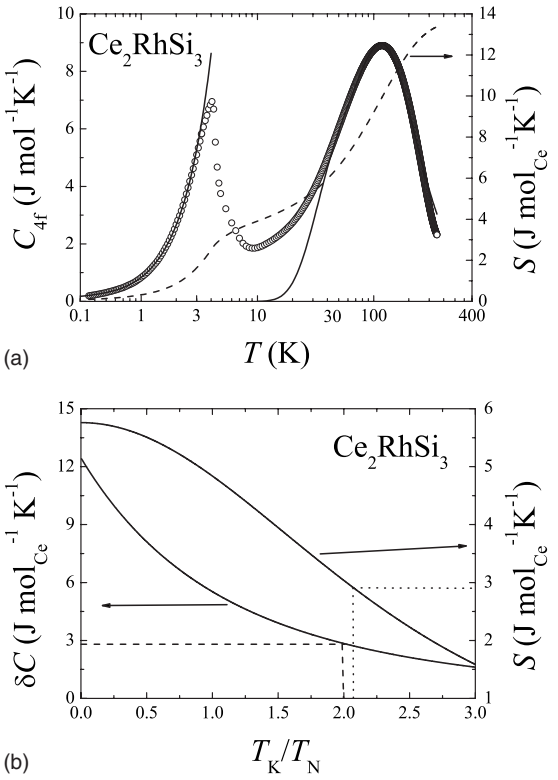

FIG. 7. (Upper panel) Temperature variations of the nonphonon contribution to the heat capacity of Ce_2RhSi_3 (left-hand side axis) and the related magnetic entropy (dashed line; right-hand side axis). Solid lines represent the Schottky and magnon contributions discussed in the text. (Lower panel) Illustration of the methods used for estimating the Kondo temperature (for explanation, see text).

cal for antiferromagnets. It is worth to note that this behavior is observed also in fields stronger than $B_c=1.5$ T, which supports the above-formulated conjecture of B_c being a critical field for the reorientation of antiparallel aligned magnetic moments rather than for a metamagnetic phase transformation. The latter transition presumably occurs near 6 T, as for this field the peak in $C(T)$ is superimposed on a broad hump that may signal the appearance of field-induced ferromagnetic state. Eventually, in a field of 8 T, the specific heat measured with $B\|c$ shows a smeared maximum characteristic of metamagnets above their metamagnetic critical field.

In contrast to the above-described behavior, the heat capacity measured in magnetic field applied along the c direction is hardly affected by field. The maximum in $C(T)$ shifts only faintly toward lower temperatures and its magnitude is almost unchanged up to 4 T. This behavior is consistent with the magnetic structure of Ce_2RhSi_3 in which the magnetic moments are aligned perpendicular to the c axis and the magnetic anisotropy in the ordered state is very large.

Assuming that the phonon contribution to the specific heat of La_2RhSi_3 is a good approximation of that in Ce_2RhSi_3, the specific heat due to $4f$ electrons in the latter compound was extracted as follows:

$$C_{4f}(T) = C(\mathrm{Ce_2RhSi_3}) - C(\mathrm{La_2RhSi_3}). \tag{2}$$

As displayed in Fig. 7, $C_{4f}(T)$ is dominated at high temperatures by a pronounced broad maximum that manifests the Schottky contribution due to crystal-field splitting of the $^2F_{5/2}$ ground multiplet of Ce^{3+} ions into three Kramers doublets. In the unit cell of Ce_2RhSi_3 there are two inequivalent sites for Ce atoms with the multiplicity 1 for Ce1 and 3 for Ce2. Applying the standard Schottky formula with the proper weights one obtains fairly good description of the experimental data above ca. 40 K (note the solid line in Fig. 7). The so-derived energies of the excited crystal-field levels are $\Delta_{11}=350$ K and $\Delta_{12}=399$ K for the Ce1 ion and $\Delta_{21}=136$ K and $\Delta_{22}=384$ K for the Ce2 ion. For both ions the total crystal-field splitting is consistent with the magnetic entropy estimated by integrating the C_{4f}/T data, which tends at high temperatures to a value of 15 J mol^{-1} K^{-1} that corresponds to the sixfold degeneracy of the $^2F_{5/2}$ multiplet.

In the ordered region, the heat capacity of Ce_2RhSi_3 is dominated by the magnetic contribution due to antiferromagnetic spin waves. Assuming that the magnon dispersion can be approximated by the relation $\omega=\sqrt{\Delta_{\mathrm{SW}}^2+Dk^2}$, in which Δ_{SW} is a gap in the spin-wave spectrum and D stands for the spin-wave stiffness, the specific heat can be expressed as[31,32]

$$C_{\mathrm{mag}} = \gamma T + c\Delta_{\mathrm{SW}}^{7/2}\sqrt{T}e^{-\Delta_{\mathrm{SW}}/T}\left[1+\frac{39T}{20\Delta_{\mathrm{SW}}}+\frac{51}{32}\left(\frac{T}{\Delta_{\mathrm{SW}}}\right)^2\right], \tag{3}$$

where the first term accounts for the electronic contribution to the specific heat, while the coefficient c is related to the spin-wave stiffness D as $c\propto D^{-3}$. The least-squares fit of Eq. (3) to the experimental data below 3 K yielded the parameters $\gamma=580$ mJ mol^{-1} K^{-2}, $c=98$ mJ mol^{-1} K^{-4}, and $\Delta_{\mathrm{SW}}=2.4$ K. The value of γ is strongly enhanced and likely indicates strong electronic correlations. In turn, the obtained spin-wave gap Δ_{SW} is of the order of magnitude often found in cerium intermetallics with antiferromagnetic ground states.

In antiferromagnetic Kondo systems the specific-heat jump at the Néel temperature, δC, is related to the characteristic Kondo temperature T_K via the formula[33,34]

$$\delta C = \frac{6k_B}{\psi''\left(\frac{1}{2}+\zeta\right)}\left[\psi'\left(\frac{1}{2}+\zeta\right)+\zeta\psi''\left(\frac{1}{2}+\zeta\right)\right]^2, \tag{4}$$

where $\zeta=(T_K/T_N)/2\pi$, while ψ', ψ'', and ψ''' are the first three derivatives of the digamma function. This universal relation is shown in the lower panel in Fig. 7. For Ce_2RhSi_3 δC is about 2.8 J mol$_{\mathrm{Ce}}^{-1}$ K^{-1}, which yields an estimate for T_K being equal to about 9 K.

Another estimate of the Kondo temperature can be derived from the value of the magnetic entropy released at T_N. From the theoretical expression[35]

$$S(T_K/T_N) = R\left(\ln[1+\exp(-T_K/T_N)]+\frac{T_K}{T_N}\frac{\exp(-T_K/T_N)}{1+\exp(-T_K/T_N)}\right) \tag{5}$$

and the experimentally determined $S(T_N)=2.8$ J mol$_{\mathrm{Ce}}^{-1}$ K^{-1}, the Kondo temperature of 9.5 K (see the lower panel in Fig.

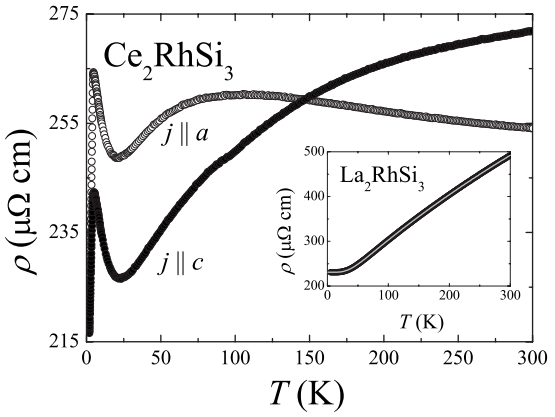

FIG. 8. Temperature dependencies of the electrical resistivity of Ce_2RhSi_3 measured with the current flowing along two characteristic directions. Inset presents the resistivity of polycrystalline La_2RhSi_3. Solid line is a BGM fit described in the text.

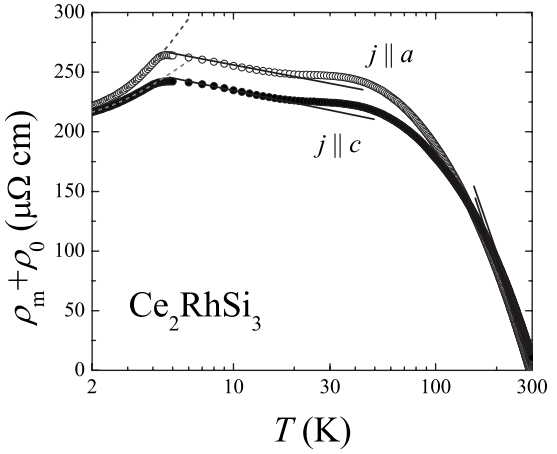

FIG. 9. Temperature variations of the magnetic contributions to the resistivity of Ce_2RhSi_3 (enlarged by the residual resistivity) for the current flowing along the a and c axes. Solid lines mark the logarithmic slopes of the resistivity in the paramagnetic state. Dashed lines represent the magnon contributions.

7) is found, in very good agreement with the value estimated from δC.

D. Electrical resistivity

The temperature variations of the electrical resistivity of single-crystalline Ce_2RhSi_3, ρ^a and ρ^c, measured along the crystallographic a and c axes, respectively, are shown in Fig. 8. At room temperature $\rho^a=254$ $\mu\Omega$ cm and $\rho^c=272$ $\mu\Omega$ cm. In both directions the resistivity changes only slightly with decreasing temperature, dropping to 222 $\mu\Omega$ cm and 217 $\mu\Omega$ cm, respectively, at 2 K. The antiferromagnetic phase transition manifests itself as sharp maxima in $\rho^a(T)$ and $\rho^c(T)$. Above $T_N=4.5$ K both components exhibit negative temperature coefficients up to about 25 K, where local minima are observed. At higher temperature ρ^c increases in a semimetallic manner up to room temperature showing only a faint hump in the vicinity of 100 K. In turn, $\rho^a(T)$ shows a broad maximum near 100 K followed by a decrease with rising temperature toward 300 K. The observed features likely reflect interplay of Kondo and crystal-field interactions.

The inset to Fig. 8 displays the electrical resistivity data for La_2RhSi_3. The $\rho(T)$ curve of this nonmagnetic isostructural analog to Ce_2RhSi_3 can be well described by a Bloch-Grüneisen-Mott (BGM) relation

$$\rho(T) = \rho_0 + \rho_{\mathrm{BGM}} = \rho_0 + 4R\Theta_R\left(\frac{T}{\Theta_R}\right)^5 \int_0^{\Theta_R/T} \frac{x^5 dx}{(e^x-1)(1-e^{-x})} - KT^3, \quad (6)$$

where ρ_0 is the residual resistivity due to lattice defects, the second term accounts for electron-phonon interactions, and the third one describes the contribution due to Mott's s-d interband scattering. Least-squares fitting of the BGM formula to the experimental data in the entire temperature range covered yielded the values $\rho_0=230$ $\mu\Omega$ cm, $\Theta_R=228$ K, $R=0.96$ $\mu\Omega$ cm K^{-1}, and $K=0.6\times10^{-7}$ $\mu\Omega$ cm K^{-3}. The parameter Θ_R is usually considered as an approximation of the Debye temperature. For La_2RhSi_3 the specific-heat data yielded $\Theta_D=247$ K, which is indeed close to Θ_R derived from the resistivity.

In order to analyze the magnetic contribution to the electrical resistivity of Ce_2RhSi_3 it was assumed that the phonon contribution in this compound can be properly approximated by that in La_2RhSi_3, i.e.,

$$\rho(T) = \rho_0 + \rho_{\mathrm{BGM}} + \rho_m. \quad (7)$$

With this assumption the temperature variations of $\rho_m^a+\rho_0$ and $\rho_m^c+\rho_0$ were derived, as displayed in Fig. 9 (note a semilogarithmic scale). In the paramagnetic region both curves show a behavior typical for the interplay of Kondo screening and crystal-field interactions.[36] In both directions the regions of logarithmic decrease of the resistivity are separated by a weak maximum related to the splitting between the crystal-field levels. According to Ref. 36, the logarithmic slopes c_K^{LT} and c_K^{HT} in the low-temperature and high-temperature ranges, respectively, are proportional to the squared effective degeneracy of the thermally populated levels: $c_K \propto \lambda^2 - 1$. In the case of Ce^{3+} ion placed in a noncubic symmetry the ground multiplet splits into three doublets, and hence for cerium compounds the expected ratio $c_K^{\mathrm{LT}}:c_K^{\mathrm{HT}}$ is 3:35. For Ce_2RhSi_3 that ratio is about 3:40 for both directions of the current, i.e., it is very close to the theoretical prediction.

Below the Néel temperature the resistivity drops rapidly due to strong decrease in spin-disorder scattering in the magnetically ordered state. In this region, the ρ_m^a and ρ_m^c curves of Ce_2RhSi_3 can be described by the formula[31,37]

$$\rho(T) = \rho_0 + b\Delta_{\mathrm{SW}}^2\sqrt{\frac{T}{\Delta_{\mathrm{SW}}}}e^{-\Delta_{\mathrm{SW}}/T}\left[1 + \frac{2\Delta_{\mathrm{SW}}}{3T} + \frac{2}{15}\left(\frac{\Delta_{\mathrm{SW}}}{T}\right)^2\right], \quad (8)$$

which takes into account scattering processes of conduction electrons on the antiferromagnetic spin waves. In this expression the same dispersion relation of magnons was assumed

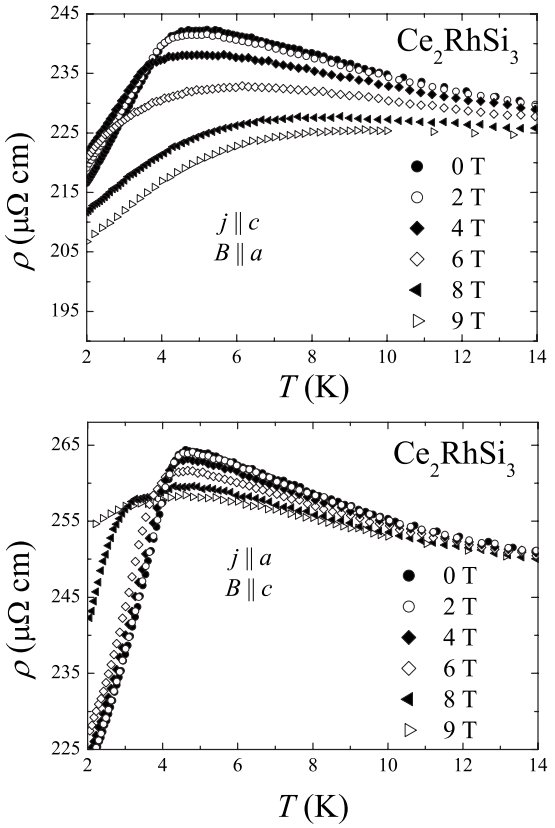

FIG. 10. Low-temperature variations of the electrical resistivity of Ce_2RhSi_3, measured along the c axis (upper panel) and the a axis (lower panel) in magnetic field applied in the a direction and the c direction, respectively.

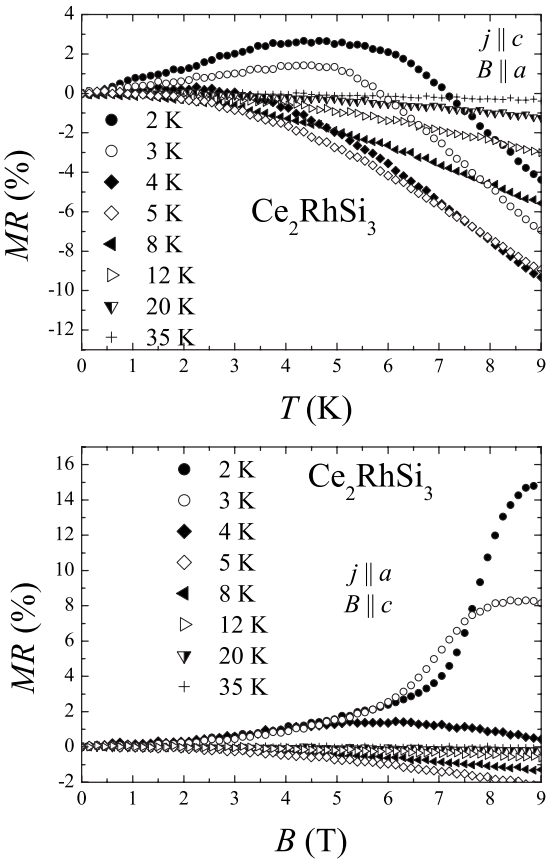

FIG. 11. Transverse magnetoresistivity isotherms of Ce_2RhSi_3, taken at several different temperatures in the antiferromagnetic and paramagnetic regions with the configurations of the electrical current and the magnetic field as in Fig. 10.

as that applied above in the analysis of the specific-heat data. Accordingly, the coefficient b was defined as $b \propto D^{-3/2}$. Least-squares fitting of this formula to the experimental data below 4.5 K gave the following parameters: $\rho_0 = 216\ \mu\Omega$ cm, $\Delta_{SW} = 8$ K, and $b = 2.9\ \mu\Omega$ cm K^{-2} for the current flowing along the a axis and $\rho_0 = 210\ \mu\Omega$ cm, $\Delta_{SW} = 6.4$ K, and $b = 2.2\ \mu\Omega$ cm K^{-2} for the current flowing along the c axis. It is worthwhile noting that the so-derived values of the spin-wave gap in Ce_2RhSi_3 is larger than that estimated from the specific-heat data (see Sec. III C), yet at least of the same order of magnitude.

E. Magnetoresistivity

The temperature dependencies of the low-temperature resistivity measured in magnetic field applied perpendicular to the flowing electrical current are presented in Fig. 10. For B directed along the a axis, which is the easy magnetization direction (see above), the maximum in $\rho^c(T)$, associated with the onset of the antiferromagnetic state, initially moves toward lower temperatures with rising the field strength but in fields stronger than 4 T this tendency is reversed. At the same time one observes a distinct broadening of the resistivity maximum. Hence, the overall behavior of $\rho^c(T)$ in $B \| a$ mimics that of the magnetic susceptibility and the heat capacity measured in the same direction of the applied magnetic field, and can be easily understood in terms of a metamagnetic phase transition that takes place between 4 and 6 T. Further support for this scenario comes from the inspection of the field variations of the transverse magnetoresistivity, MR $= \frac{\rho(B)-\rho(0)}{\rho(0)}$, measured with $j \| c$ and $B \| a$. As shown in the upper panel in Fig. 11, in the ordered region, magnetoresistivity (MR) is positive in low fields and increases with rising field. Then it goes through a broad maximum (3% at 2 K in a field of 6 T) and subsequently decreases becoming negative in higher fields. With increasing temperature the maximum in MR moves toward lower fields and its magnitude diminishes. Such a behavior is characteristic of antiferromagnets undergoing a metamagnetic phase transition. The value of the metamagnetic critical field, associated with the maximum in MR, corresponds well with that derived from the magnetization and heat-capacity data (compare Figs. 4 and 6).

For the magnetic field applied along the c axis the low-temperature resistivity measured in the a direction remains nearly unchanged up to 4 T (see the lower panel in Fig. 10). In stronger fields, the maximum in $\rho^a(T)$ moves toward lower temperatures, accompanied by some broadening and decrease in its magnitude. In fields of 8 and 9 T a new feature in $\rho^a(T)$ is observed in the form of another maximum that likely manifests some field-induced change in the magnetic structure of the compound investigated. This latter conjecture seems corroborated by the magnetoresistivity data collected with $j \| a$ and $B \| c$, displayed in the lower panel in

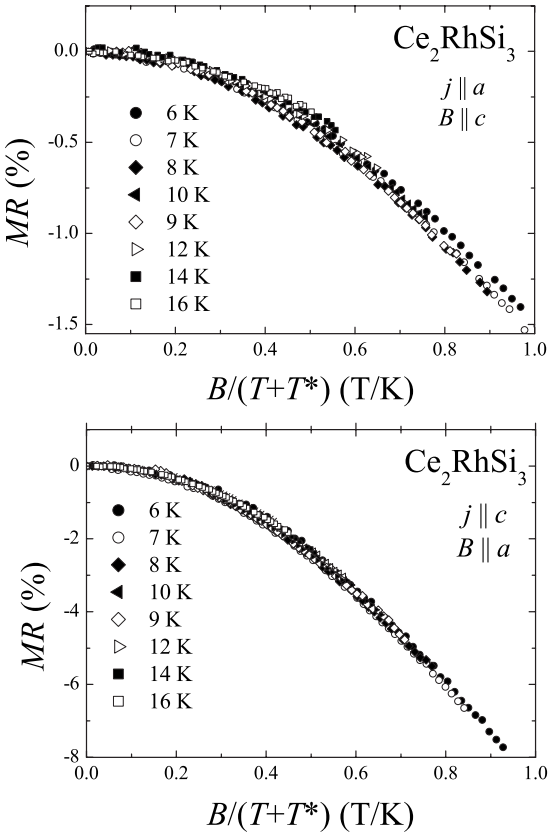

FIG. 12. Schlottmann scaling of the paramagnetic magnetoresistivity isotherms of Ce_2RhSi_3 presented in Fig. 11.

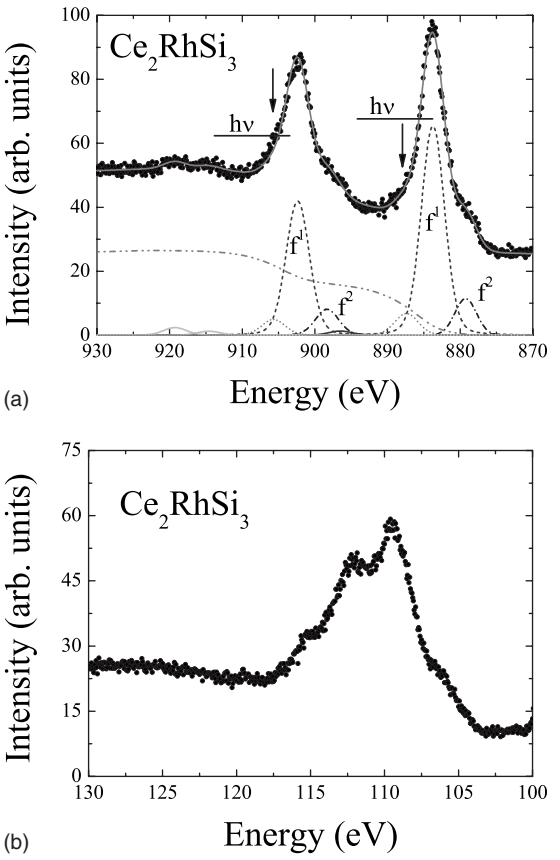

FIG. 13. Ce $3d$ (upper panel) and Ce $4d$ (lower panel) XPS spectra obtained for Ce_2RhSi_3. The f^1 and f^2 components were separated on the basis of the Doniach-Šunjić theory. Plasmon resonance structures are indicated by the horizontal lines (plasmon energy $h\nu \approx 13$ eV). Vertical arrows point to the shoulders originating from small amount of Ce_2O_3 on surface of the specimen measured.

Fig. 11. Below the Néel temperature, MR is positive and increases with increasing field up to 6 T, as expected for an antiferromagnet. In stronger fields, MR measured at 2 K shows a rapid rise to reach about 15% in 9 T. The isotherms taken at higher temperatures exhibit a metamagneticlike maximum that shifts toward smaller fields and diminishes in its height with rising temperature.

In the paramagnetic region, the transverse magnetoresistivity, measured in both above-defined configurations of the current and the magnetic field with respect to the crystallographic axes, is negative and exhibits a field dependence that is reminiscent of the behavior of Kondo systems. In 9 T, MR measured with $j \| c$ and $B \| a$ reaches just above T_N a value of –9%, while for $j \| a$ and $B \| c$ it is does not exceed 2%. As is apparent from Fig. 12, for both configurations the paramagnetic isotherms can be superimposed onto each other using the single-ion Kondo scaling relation $\mathrm{MR}(B) = f[B/(T+T^*)]$, derived within the Bethe-Ansatz approach.[38] The characteristic temperatures T^*, which ensure the best overlap of the MR curves, are 3.7 K for ρ^c with $B \| a$ and 1.7 K for ρ^a with $B \| c$.

F. Electronic structure

Ce core-level x-ray photoemission spectroscopy (XPS) is an appropriate method to get insight into the character of the Ce $4f$ states in Ce-based intermetallics owing to the strong Coulomb interaction between the photoemission core hole and the electrons located near the Fermi level. The spin-orbit (SO) interaction results in two sets of photoemission lines in such XPS spectra, which are, respectively, assigned to the $3d_{3/2}$ and $3d_{5/2}$ components of the final states. Each SO set of the Ce $3d$ lines may consist of three contributions.[39] The main peaks $3d^9f^1$ originate from Ce^{3+}. The $3d^9f^0$ components, ~11 eV away from the f^1 peaks, originate from Ce^{4+}. In turn, the $3d^9f^2$ final-state components appear when the core hole becomes screened by an additional $4f$ electron due to the hybridization of the Ce $4f$ shell with the conduction band. Consequently, the contribution of the $3d^9f^2$ lines in the measured Ce $3d$ spectrum, located on the low-energy side of the main lines at the distance of ~4 eV, reflects the hybridization strength $\delta = \pi V^2 N(\epsilon_F)$.

The upper panel in Fig. 13 shows the Ce $3d$ XPS spectrum of single-crystalline Ce_2RhSi_3, where a background, calculated using the Tougaard algorithm,[40] was subtracted from the measured XPS data. The separation of the overlapping peaks in the spectrum was done on the basis of the Doniach-Šunjić theory.[41] In order to estimate the hybridization strength between the $4f$ states and the conduction band a quantitative analysis of these data was made based on the Gunnarsson and Schönhammer model[39] (for details of the applied approach, see Ref. 42). The hybridization parameter

δ found for Ce_2RhSi_3 is about 80 meV that is a value typical for Ce-based intermetallics with stable valence of cerium ions. In the spectrum presented in Fig. 13 there are no distinct intensities at a distance of ~11 eV from the main photoemission lines which could be assigned to the Ce $3d^9f^0$ final states (some tiny features observed at the binding energies of 896 and 915 eV are probably plasmons associated with group oscillations of the conduction electrons). This finding corroborates the presumption of well-defined trivalent character of the Ce ions.

Another evidence of the stable valence of the Ce ions in Ce_2RhSi_3 may be provided by the Ce 4*d* XPS spectrum, displayed in the lower panel in Fig. 13. The multiplet structure observed for the binding energies ranging between 104 and 118 eV can be assigned to the $4d^9f^1$ final states, while no additional peaks are seen at higher binding energies, which would indicate the Ce $4d^9f^0$ state.[39] The shapes of 4*d* XPS peaks are strongly affected by multiplet effects, which should be treated in intermediate coupling regime.[39] For this reason, their quantitative analysis is not straightforward and not attempted here. Nevertheless, the observed 4*d* spectrum seems fully consistent with that of the Ce 3*d* states. Thus, the XPS results support the magnetic-susceptibility and heat-capacity data that also indicated the presence of stable Ce^{3+} ions.

IV. SUMMARY

The Czochralski grown single crystal of Ce_2RhSi_3 was found to form in a derivative of the AlB_2-type structure, characterized by doubling the unit cell along the basal hexagonal lattice parameter *a*, while leaving the *c* parameter unaltered. This finding is at odds with the crystal structure hitherto considered in the literature, which was assigned to Ce_2RhSi_3 presuming that it is isostructural with Er_2RhSi_3 (for the latter compound both lattice parameters are doubled with respect to the AlB_2-type[19,28]). Most importantly, the refined unit cell of Ce_2RhSi_3 exhibits full crystallographic ordering of all the constituent atoms.

Based on this feature, by analogy with other R_2TM_3 phases, one may expect that the compound orders magnetically at low temperatures. The detailed bulk magnetic, electrical, and thermodynamic measurements of single-crystalline samples indeed indicated long-range antiferromagnetic order that sets in at T_N=4.5 K. This result corroborates the previous findings reported for polycrystals of Ce_2RhSi_3, however the Néel temperature is considerably lower than the literature data.[21,23–25] This discrepancy might be due to some deviations in the composition of the polycrystalline samples from the ideal stoichiometry (note that the refinements revealed the single crystal studied in the present work to have full atomic occupancies at all the sites) or it may be related to a crystal structure different from that determined for the single crystal.

The antiferromagnetic unit cell of Ce_2RhSi_3 consists of the magnetic moments carried by two crystallographically inequivalent cerium atoms, which are confined to the hexagonal basal plane. The magnetic structure likely changes in a field of 1.5 T applied along the easy magnetization direction, yet it remains antiferromagnetic in character up to at least 4 T. In stronger fields a field-induced ferromagnetism is observed. For magnetic field applied along the other direction a metamagnetic phase transition is not observed below 8 T. This finding indicates a strong magnetocrystalline anisotropy in Ce_2RhSi_3 that is rather uncommon for Ce-based compounds. Obviously, the conjecture on field-induced changes in the magnetic structure being the origin of the observed features in the magnetization, heat capacity, and electrical resistivity of the silicide studied should be verified by neutron diffraction performed in external magnetic field.

The large negative paramagnetic Curie temperature, negative logarithmic slopes of the magnetic contribution to the resistivity, as well as strongly enhanced low-temperature specific heat are all indicative that Ce_2RhSi_3 belongs to a family of dense Kondo systems with heavy-fermion ground state. Using different approaches, the Kondo temperature was estimated to be about 9 K. Moreover, in the paramagnetic region the magnetic, electrical transport, and thermal behaviors of the compound investigated are governed by strong crystal-field interactions with large energy separation between the ground state and the first-excited state (as much as about 350 K for the Ce1 ion and 140 K for the Ce2 ion) and the overall energy splittings of the order of 400 K. An inelastic neutron-scattering experiment is required to prove the crystalline electric field model worked out in this study. Some *ab initio* crystal-field and electronic structure calculations are presently underway to complement the present discussion based on the experimental data. Those results will be published in a separate extensive article.

ACKNOWLEDGMENTS

The authors are grateful to Daniel Gnida for his assistance with resistivity measurements. This work was supported by the Ministry of Science and Higher Education within Research Project No. N202 116 32/3270. Part of the research was performed in the frame of the National Network "Strongly correlated materials: preparation, fundamental research and applications." The authors thank the Wroclaw Centre for Networking and Computing for access to the MATLAB license (Grant No. 92).

*On leave from Department of General and Inorganic Chemistry, Volyn State University, 43025 Lutsk, Ukraine.

[1] K. Yubuta, T. Yamamura, and Y. Shiokawa, J. Phys.: Condens. Matter **18**, 6109 (2006).

[2] C. Tien, C. H. Feng, C. S. Wur, and J. J. Lu, Phys. Rev. B **61**, 12151 (2000).

[3] D. P. Rojas, L. C. J. Pereira, E. B. Lopes, J. C. Waerenborgh, L. M. da Silva, F. G. Gandra, and A. N. Medina, J. Alloys Compd.

432, 34 (2007).
[4] B. Chevalier, R. Pöttgen, B. Darriet, P. Gravereau, and J. Etourneau, J. Alloys Compd. **233**, 150 (1996).
[5] D. X. Li, S. Nimori, Y. Shiokawa, Y. Haga, E. Yamamoto, and Y. Onuki, Phys. Rev. B **68**, 172405 (2003).
[6] D. X. Li, A. Donni, Y. Kimura, Y. Shiokawa, Y. Homma, E. Y. Y. Haga, T. Honma, and Y. Onuki, J. Phys.: Condens. Matter **11**, 8263 (1999).
[7] M. Pinto, Acta Crystallogr. **21**, 999 (1966).
[8] D. Kaczorowski and H. Noël, J. Phys.: Condens. Matter **5**, 9185 (1993).
[9] R. Pöttgen, P. Gravereau, B. Darriet, B. Chevalier, E. Hickey, and J. Etourneau, J. Mater. Chem. **4**, 463 (1994).
[10] R. A. Gordon, C. J. Warren, M. G. Alexander, F. J. DiSalvo, and R. Pöttgen, J. Alloys Compd. **248**, 24 (1997).
[11] N. Takeda and M. Ishikawa, J. Phys. Soc. Jpn. **67**, 1062 (1998).
[12] S. Majumdar, M. M. Kumar, R. Mallik, and E. V. Sampathkumaran, Solid State Commun. **110**, 509 (1999).
[13] S. Majumdar and E. V. Sampathkumaran, Phys. Rev. B **62**, 8959 (2000).
[14] S. Majumdar, M. M. Kumar, R. Mallik, and E. V. Sampathkumaran, Physica B **281-282**, 367 (2000).
[15] T. Yamamura, D. X. Li, K. Yubuta, and Y. Shiokawa, J. Alloys Compd. **408-412**, 1324 (2006).
[16] R. Mallik and E. V. Sampathkumaran, J. Magn. Magn. Mater. **164**, L13 (1996).
[17] A. Szytuła, M. Hofmann, B. Penc, M. Slaski, S. Mujumdar, E. Sampathkumaran, and A. Zygmunt, J. Magn. Magn. Mater. **202**, 365 (1999).
[18] S. R. Saha, H. Sugawara, T. D. Matsuda, Y. Aoki, H. Sato, and E. V. Sampathkumaran, Phys. Rev. B **62**, 425 (2000).
[19] B. Chevalier, P. Lejay, J. Etourneau, and P. Hagenmuller, Solid State Commun. **49**, 753 (1984).
[20] A. Szytuła, J. Leciejewicz, and K. Małetka, J. Magn. Magn. Mater. **118**, 302 (1993).
[21] J. Leciejewicz, N. Stüsser, A. Szytuła, and A. Zygmunt, J. Magn. Magn. Mater. **147**, 45 (1995).
[22] W. Bażela, E. Wawrzyńska, B. Penc, N. Stüsser, A. Szytuła, and A. Zygmunt, J. Alloys Compd. **360**, 76 (2003).
[23] I. Das and E. V. Sampathkumaran, J. Magn. Magn. Mater. **137**, L239 (1994).
[24] T. Nakano, K. Sengupta, S. Rayaprol, M. Hedo, Y. Uwatoko, and E. V. Sampathkumaran, J. Phys.: Condens. Matter **19**, 326205 (2007).
[25] S. Patil, K. K. Iyer, K. Maiti, and E. V. Sampathkumaran, Phys. Rev. B **77**, 094443 (2008).
[26] G. Sheldrick, *shelxs-97 and shelxl-97, Programs for Crystal Structure Refinement* (University of Göttingen Press, Göttingen, Germany, 1997).
[27] J. Rodriguez-Carvajal, Physica B **192**, 55 (1993).
[28] R. E. Gladyshevskii, K. Cenzual, and E. Parthe, J. Alloys Compd. **189**, 221 (1992).
[29] U. C. Rodewald, R.-D. Hoffmann, R. Pöttgen, and E. V. Sampathkumaran, Z. Naturforsch., B: Chem. Sci. **58**, 971 (2003).
[30] E. S. R. Gopal, *Specific Heats at Low Temperatures* (Plenum, New York, 1996).
[31] S. N. de Medeiros, M. A. Continentino, M. T. D. Orlando, M. B. Fontes, E. M. Baggio-Saitovitch, A. Rosch, and A. Eichler, Physica B **281-282**, 340 (2000).
[32] M. A. Continentino, S. N. de Medeiros, M. T. D. Orlando, M. B. Fontes, and E. M. Baggio-Saitovitch, Phys. Rev. B **64**, 012404 (2001).
[33] C. D. Bredl, F. Steglich, and K. D. Schotte, Z. Phys. B **29**, 327 (1978).
[34] J. A. Blanco, M. de Podesta, J. I. Espeso, J. C. Gomez Sal, C. Lester, K. A. McEwen, N. Patrikios, and J. Rodriguez Fernandez, Phys. Rev. B **49**, 15126 (1994).
[35] H. Yashima, H. Mori, N. Sato, and T. Satoh, J. Magn. Magn. Mater. **31-34**, 411 (1983).
[36] B. C. D. Cornut, Phys. Rev. B **5**, 4541 (1972).
[37] M. B. Fontes, J. C. Trochez, B. Giordanengo, S. L. Budko, D. R. Sanchez, E. M. Baggio-Saitovitch, and M. A. Continentino, Phys. Rev. B **60**, 6781 (1999).
[38] P. Schlottmann, Phys. Rep. **181**, 1 (1989).
[39] J. C. Fuggle, F. U. Hillebrecht, Z. Żołnierek, R. Lasser, C. Freiburg, O. Gunnarsson, and K. Schonhammer, Phys. Rev. B **27**, 7330 (1983).
[40] S. Tougaard and P. Sigmund, Phys. Rev. B **25**, 4452 (1982).
[41] S. Doniach and M. Šunjić, J. Phys. C **3**, 285 (1970).
[42] A. Ślebarski, T. Zawada, J. Spałek, and A. Jezierski, Phys. Rev. B **70**, 235112 (2004).